Technical University of Denmark

DTU

Oxidative trends of TiO2—hole trapping at anatase and rutile surfaces

Zawadzki, Pawel; Laursen, Anders Bo; Jacobsen, Karsten Wedel; Dahl, Søren; Rossmeisl, Jan

DTU Library
Technical Information Center of Denmark

Dynamic Article Links ▶

PAPER

Oxidative trends of TiO$_2$—hole trapping at anatase and rutile surfaces†

Paweł Zawadzki,‡*^{a} Anders B. Laursen,^{b} Karsten Wedel Jacobsen,^{a} Søren Dahl^b and Jan Rossmeisl^a

Understanding the nature of photogenerated carriers in a photocatalyst is central to understanding its photocatalytic performance. Based on density functional theory calculation we show that for TiO$_2$, the most popular photo-catalyst, the electron hole self-trapping leads to band gap states which position is dependent on the type of surface termination. Such variations in hole state energies can lead to differences in photocatalytic activity among rutile and anatase surface facets. We find that the calculated hole state energies correlate with photo-deposition and photo-etching rates. We anticipated that our results can aid the design of more reactive photo-catalysts based on TiO$_2$ and our approach can be utilized for other relevant photo-catalysts as well.

1 Introduction

Photo-catalysis is presently used in a large variety of applications such as water and air purification, self-cleaning surfaces, and anti-fogging coatings. Furthermore, for future sustainable fuel production from solar light efficient photo-catalysis is crucial.[1] Titanium dioxide is the most popular photocatalyst as it is technologically a very attractive material—abundant, harmless, and chemically inert. Many aspects of TiO$_2$ photo-catalysis however still remain obscure.[2,3] Understanding the influence of TiO$_2$ morphology on the photocatalytic activity is especially important as such effects can be exploited in photo-catalyst design.

Based on density functional theory calculation we show that differences in photocatalytic activity can arise due to morphology dependent variation of spacial and energetic distribution of hole trapping states.

2 Surface hole trapping

Hole trapping states in TiO$_2$ have been observed in many experiments including electron paramagnetic resonance (EPR), transient absorption spectroscopy (TAS), and photo-luminescence (PL) (for a review see Fujishima *et al.*[2] and Henderson[3]) but their exact nature remained unclear. Only recently it has become more evident that holes in TiO$_2$ self-trap forming O$^-$ small polarons[4–9]—an electronic hole localized on an oxygen

lattice site surrounded by a deformed lattice. The hole trapping state is formed by an oxygen p-like orbital perpendicular to the flat OTi$_3$ building blocks of TiO$_2$. Our DFT calculation predicted that trapping in anatase is stronger than in rutile and the small-polaron stabilisation energy with respect to the delocalized holes in the valence band (VB) is 0.2 eV; in rutile the two types of hole states have comparable stability.[5] Di Valentin *et al.* found a trapping strength of 0.75 eV in anatase.[7] Here we focus on the effect of surface termination on the trapping strength as this issue is particularly relevant to the understanding of the TiO$_2$ photo-catalysis.

A surface, like any other crystal imperfection, induces lattice relaxation and charge redistribution. These processes create potential variations in surface layers. The localized nature of trapped hole states makes their energetics highly sensitive to such potential changes. In Fig. 1 we show a schematic energy diagram

^{a}Center for Atomic-Scale Materials Design, Department of Physics, Technical University of Denmark, DK-2800 Kgs. Lyngby, Denmark. E-mail: Pawel.Zawadzki@nrel.gov
^{b}Center for Individual Nanoparticle Functionality, Department of Physics, Technical University of Denmark, DK-2800 Kgs. Lyngby, Denmark
† Electronic supplementary information (ESI) available. See DOI: 10.1039/c2ee22721e
‡ Present address: National Renewable Energy Laboratory, Golden, Colorado 80401, USA.
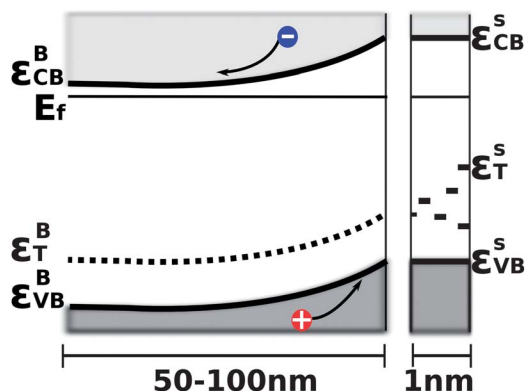
Fig. 1 Energy diagram for an n-type semiconductor with upward band banding. Hole self-trapping energies ε_T are sensitive to potential variations in surface layers of $\approx$1 nm thickness. ε_{CB} and ε_{VB} are the valence band and the conduction band edges, respectively; superscripts S and B denote surface and bulk values, respectively.

of a surface terminated semiconductor with upward bended bands. The hole trapping level ε_T (dashed line) is located in the band gap and in the same way as the VB and the conduction band (CB) edges follow the space charge potential. At the very surface layers, however, crystal structure interruption gives rise to potential variations that modify the stability of the trapped (localized) hole states.

In Fig. 2 we plot such energy diagrams for anatase {001} and {011} surfaces (for anatase {100} and rutile {001}, {011}, {110}, {100} see Fig. S1–4 in the ESI†). The hole stabilisation energy (the trapping level) oscillates along the surface layers giving rise to surface and sub-surface small-polaron states. For most terminations the hole stabilisation energy is the largest at the surface oxygen bridge site (O$\langle$). This site is two-fold coordinated by Ti cations, therefore a positive hole charge is less destabilized compared to three-fold coordinated bulk or surface in-plane
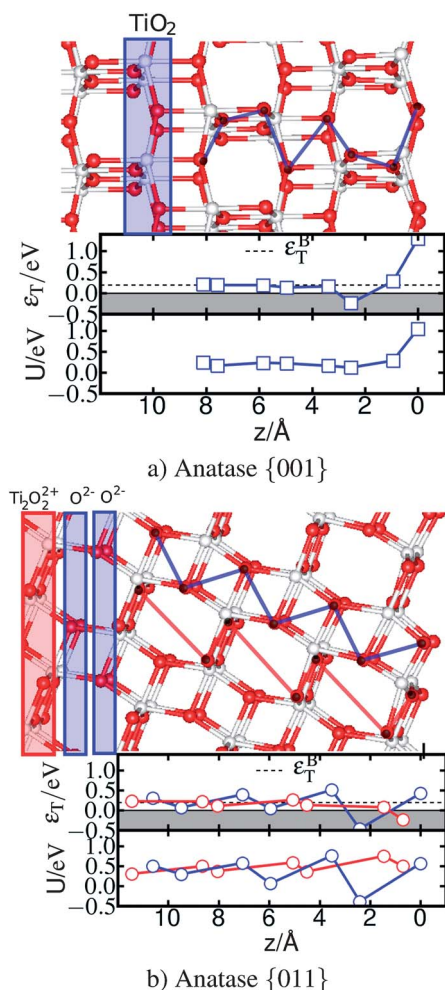
oxygen sites (–O$\langle$). We note here that the active role of bridging oxygen sites in photo-oxidation mechanisms is supported by isotope labeling experiments.[10,11]

For surfaces composed of charged layers, such as anatase {011} formed by $[O^{2-}(TiO)_2^{4+}O^{2-}]_n$, the energy strongly oscillates around the bulk value. For neutral layer stacking, as in the case of anatase {001} composed of $[TiO_2]_n$, the trapping strength is more even and only the strengths of the surface trapping sites are significantly modified. Moreover, for some surfaces there are two possible hole orbital alignments with respect to the surface. For instance, for anatase {011} the lobe of the hole orbital can be parallel or nearly perpendicular to the surface. In the former case the hole stability oscillates more strongly (blue circles in Fig. 2) than in the latter case.

These observations suggest the electrostatic potential in the surface layers to be responsible for the variation of the trapping strength. To check our presumption we construct a similar depth profile for the electrostatic energy $U(z) = \int V(r)n_p(r-z)\mathrm{d}r$ (see the bottom plots in Fig. 2) where $V(r)$ is the electrostatic potential, and $n_p(r-z)$ is the charge density of the oxygen atomic p orbital centered at the oxygen lattice site at depth z. Similarities between $U(z)$ and $\varepsilon_T(z)$ are clear. A stronger $U(z)$ variation in the case of hole states with the orbital parallel to the surface arises because the overlap of the hole density with the electrostatic potential changes is larger than when the orbital is perpendicular to the surface. The perpendicular alignment smoothens the variation of the electrostatic potential between surface layers.

A quantity directly related to the surface electrostatic potential is the work function $\phi = (\bar{V}^B - V^V) - \mu/e$ where the difference between the average electrostatic potential in the bulk $\bar{V}^B$ and the reference value in the vacuum V^V is due to the surface dipole moment and μ is the chemical potential of the electron—a bulk property.[12] In Fig. 3 we plot the trapping strength of the hole states localized on the bridging oxygen sites ε_T^S against the work function. Intelligibly, the lower the work function the more stable the hole state is, as it is easier to remove an electron. The correlation, however, is not linear as local effects are important. Nevertheless, it is now easy to see the trends in surface hole stability: for rutile {100} < {110} < {011} < {001}; for anatase {011} < {100} < {001}.

a) Anatase {001}

b) Anatase {011}

Fig. 2 Self-trapping energies ε_T with respect to the valence band edge for anatase {001} and {011} surfaces. In surface layers hole stabilisation energies oscillate and within 1–2 nm below the surface the profiles converge to the bulk value ε_T^B. Larger hole self-trapping strength on the {001} surface compared to the {011} surface provides larger driving force for holes transport toward the {001} termination. $U(z)$ is the overlap of the electrostatic potential $V(r)$ and the density of the hole orbital $n_p(r-z)$ centered at depth z. Similarities between $U(z)$ and ε_T suggest that the variation of trapping strength in surface layers is an electrostatic effect. The shaded area denotes the valence band.
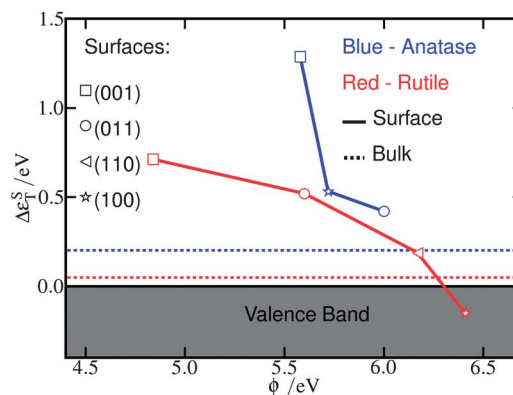

Fig. 3 Correlation between the work function ϕ and the stabilities of the self-trapped holes ε_T for the different rutile and anatase surfaces. The shaded area denotes the valence band whereas dashed lines denote the bulk self-trapping strengths ε_T^B.

Electrostatic effects also explain the instability of the hole state on rutile {100}. This surface is formed by $[Ti^{4+}O_2^{4-}]_n$ stacking (see Fig. S1 and S2 in the ESI†) and the lobe of the hole orbital is immersed in the Ti^{4+} layer that destabilizes the positive hole charge. In contrast, for the stable holes on {001} rutile and anatase surfaces the hole orbital is aligned parallel to neutral layers.

3 Hole trapping and photocatalytic activity

A successful photo-catalytic transformation of the absorbed photon energy must comprise: separation of photo-generated electron–hole pairs, carrier transport to surface active sites and finally chemical reaction. Depending on the relative kinetics of these steps the rate of the overall photocatalytic process can be limited by either of them. Charge separation and transport are fast processes and the photogenerated holes can reach the surface within picoseconds after the excitation.[13,14] Many reactions, especially those involving nuclear rearrangements, occur on much longer time scales, for instance a microsecond hole transfer to toluene or acetonitryl,[15] or millisecond–second water oxidation and oxygen evolution.[16] Therefore, in those cases the population of photogenerated carriers has sufficient time to attain a certain degree of thermal equilibrium so an increase in carrier stability on surface sites leads to an increase in carrier availability for reaction.

Since surface trapping levels, with the exception of {100} rutile, are well above the VB edge the surface hole distribution will be dominated by the trapped rather than the VB holes. Therefore if photo-generated holes are in equilibrium between themselves the trend in hole stability will translate into the surface hole density. For instance a hole stability of 1.1 eV on the anatase {001} with respect to the bulk value will enhance the equilibrium surface hole density by $p^S/p^B = \exp[(\varepsilon_T^S - \varepsilon_T^B)/k_B T] \approx 10^{20}$ at room temperature. In a non-equilibrium situation such a large driving force for hole transport to the surface enhances the electron–hole separation necessary for obtaining any photo-catalytic effect. An increase in the O^- concentration with increasing {001} surface area has been observed in the EPR experiment by D'Arienzo et al. and correlated with stronger photo-catalytic activity.[8]

The calculated hole stabilities can explain the experimentally observed photo-deposition and photo-etching rates: Bae and Ohno[17] found that for rutile nanorods terminated by {001}, {110}, and {111} planes oxidation of Pb^{2+} to PbO_2 takes place on {001} surfaces whereas reduction of $PtCl_6^{2-}$ to Pt takes place on {110} surfaces. In a similar experiment by Ohno et al. rutile {011} were more oxidative than {110} and anatase {001} were more oxidative than {011}.[18] Furthermore, in anodic photo-etching of rutile in aqueous sulfuric acid {001} and {100} planes were found to be the most and the least oxidative, respectively—TiO_2 dissolution ($TiO_2 + h^+ + HSO_4^- \rightarrow O_2 + TiHSO_4^{3+}$) occurs preferentially along the [001] direction and leads to formation of holes or grooves with {100} surfaces exposed.[11,19] These experiments allow us to order the surface facets by increasing oxidative properties: for rutile {100} < {110} < {011} < {001} and for anatase {011} < {001}—the order in which surface hole stability also increases.

A higher hole stabilisation on the most abundant anatase {110} and {100} compared to rutile {110} surfaces reflects the fact that anatase is generally more photo-catalytically active. For

most reactions self-trapped holes at the surface should be sufficiently oxidative as the VB edge in TiO_2 lays quite high on the electrochemical scale (3.0 V [NHE]).[2] For instance the hole stabilization on anatase {001} of 1.3 eV reduces the oxidative power to ca. 1.7 V [NHE] which is still sufficient for e.g., Pb^{2+} oxidation ($E^0_{PbO_2/Pb^{2+}} = 1.46$ V [NHE]). For trapped hole states in anatase Lawless et al.[20] and Tojo et al.[21] reported oxidation potentials of ca. 1.5–1.7 V [NHE] from pulse radiolysis and flash photolysis experiments, respectively. Bahnemann et al. found two types of trapped states: deeply trapped holes at ca. 1.5 V [NHE] not reacting with dichloroacetate and thiocyanate; and reactive shallowly trapped holes at higher redox potentials.[14]

Further support for the surface hole self-trapping comes from observations of shifts of the flat band potential upon light irradiation. Hagfeldt et al.[22] compared Mott–Schottky plots for TiO_2 nanocrystalline films under dark and UV-light conditions. Irradiated films showed larger capacitance and the response shifted anodically indicating the presence of high density surface hole states. Since the self-trapping centers are associated with the oxygen lattice sites, a high density of trapping states is possible and can arise at strong UV illumination. Such a high density of photo-generated surface hole states could explain a dramatic improvement of dye-sensitized solar cell performance when exposed to UV light.[23,24] The electrostatic field induced by the positive surface hole charge will decrease the Schottky barrier at the metal/TiO_2 contact and therefore facilitate electron transfer.

Self-trapping is especially important for nano-sized TiO_2 particles. There the band bending does not develop fully and the facet dependent trapping strength can be the only driving force for charge separation. Under a typical donor density $N_d = 10^{17}$ cm^{-3} in TiO_2 for a particle size of 20 nm the potential drop across the space charge layer is of the order of thermal energy[25] and thus irrelevant. Phase and morphology dependent hole self-trapping strength will also enhance charge separation in phase mixtures. Such an effect has been observed, in particular for Degussa P25,[26,27] and is attributed to charge transfer between the two TiO_2 phases.[27,28] But, there is no consensus on the direction of such transfer. We think that morphology dependent positions of surface hole (and electron) states play an important role and a simple consideration of the positions of the VB and the CB edges or the averaged work function[29,30] is not sufficient to explain synergism in TiO_2 phase mixtures.

4 Conclusion

In conclusion, we have shown that the position of the hole trapping states in the band gap varies among rutile and anatase facets. Differences in the hole trapping strengths provide a driving force for electron–hole separation and lead to the variation in facets activity toward oxidation processes and can lead to increase in the activity as long as the hole in the surface state is below the potential for the oxidation reaction the hole should perform. We think that this understanding could help to design more efficient photo-catalysts, for instance by depositing an oxidation catalyst on an appropriate surface[31] or by tuning a nano-particle shape for a better charge separation step. Furthermore, we expect that charge trapping in surface layers, which induced variations in the electrostatic potential, occurs not only in TiO_2 but also in other ionic materials.

5 Method

We performed DFT calculations within the Projector-Augmented Wave formalism implemented in the GPAW code.[32] Pseudo wave functions, densities and potentials were represented on a uniform, real-space grid with a spacing of 0.2 Å. To account for exchange-correlation (XC) effects we chose a revised Perdew–Burke–Ernzerhof (RPBE)[33] functional. The Brillouin zone was sampled with a Monkhorst–Pack mesh ensuring that $ka \geq 18$ Å where k is the number of sampling points and a is the periodicity in any direction.

We optimized the lattice parameters of rutile ($P4_2/mnm$) and anatase ($I4_1/amd$) TiO$_2$ (rutile: $a = 4.691$, $c = 2.975$, $u = 0.3061$; anatase: $a = 3.829$, $c = 9.744$, $u = 0.2062$). Calculations were performed for supercells defined through tetragonal lattice vectors, [a, b, c], of the respective crystallographic cells: For rutile {001}, {011}, {110}, and {100} surfaces we used [$a − b$, $a + b$, $8c$], [$−b + c$, $+a$, $4b + 4c$], [$2c$, $a − b$, $4(a + b)$], [b, $2c$, $5a$], respectively; For anatase {001}, {100}, and {101} we used: [$2a$, $2b$, $2c$], [$2b$, c, $4a$], [$−a + c$, $−2b$, $3a + 3c$], respectively.

To create an electron hole state we employed linear expansion Δ-self consistent field (Δ-SCF). The method allows us to add/subtract the electron density of the specified orbital at each SCF cycle. The hole state was generated by removing the electron density of the oxygen p-like orbital perpendicular to the C_{2v} symmetric OTi$_3$ unit of the TiO$_2$ structure and placing it at the bottom of the CB. With such a constraint on the electronic structure we relaxed the atomic coordinates, keeping one bottom layer of the slab fixed. To construct the hole trapping strength profiles we calculated Δ-SCF energies with the hole localized in different surface layers and shifted the energies such that at a large depth relative to the surface they converge to the hole trapping strength in the bulk equal to 0.2 eV and 0.05 eV for anatase and rutile, respectively.[5] Such an alignment is necessary to establish a common reference energy required for comparison of the hole self-tapping levels between different surface terminations.

An important issue that needs to be taken into account when approximate XC DFT is used to model localized states is the many electron self-interaction[34] or delocalization error.[35] The error is largely responsible for the biased treatment of states with different degrees of charge localization in DFT and, self-trapping energies are particularly sensitive to it as they measure the energy difference between delocalized and localized states. The self-trapping trends calculated here, however, compare relative energies between states with the same degree of charge localization, hole states localized on a single p-like orbital, thus are much less prone to the delocalization error. Only the absolute scale for the self-trapping energy is sensitive to the error. To establish such a scale we used the bulk hole self-trapping energy that was corrected for the delocalization error.[5]

The work function (of intrinsic TiO$_2$) has been calculated as a difference between the vacuum potential and the Fermi level of a symmetric slab (both surfaces relaxed) and converged with respect to the slab thickness (see ESI, Fig. S5†).

For a more detailed discussion of the procedure see ESI.†

References

1 A. Valdes, J. Brillet, M. Gratzel, H. Gudmundsdottir, H. A. Hansen, H. Jonsson, P. Klupfel, G.-J. Kroes, F. Le Formal, I. C. Man, R. S. Martins, J. K. Norskov, J. Rossmeisl, K. Sivula, A. Vojvodic and M. Zach, *Phys. Chem. Chem. Phys.*, 2012, **14**, 49.
2 A. Fujishima, X. Zhang and D. A. Tryk, *Surf. Sci. Rep.*, 2008, **63**, 515–582.
3 M. A. Henderson, *Surf. Sci. Rep.*, 2011, **66**, 185–297.
4 S. Yang, A. T. Brant and L. E. Halliburton, *Phys. Rev. B: Condens. Matter Mater. Phys.*, 2010, **82**, 035209.
5 P. Zawadzki, K. W. Jacobsen and J. Rossmeisl, *Chem. Phys. Lett.*, 2011, **506**, 42–45.
6 P. Zawadzki, J. Rossmeisl and K. W. Jacobsen, *Phys. Rev. B: Condens. Matter Mater. Phys.*, 2011, **84**, 121203.
7 C. Di Valentin and A. Selloni, *J. Phys. Chem. Lett.*, 2011, **2**, 2223–2228.
8 M. D'Arienzo, J. Carbajo, A. Bahamonde, M. Crippa, S. Polizzi, R. Scotti, L. Wahba and F. Morazzoni, *J. Am. Chem. Soc.*, 2011, **133**, 17652.
9 J. Cheng, M. Sulpizi, J. VandeVondele and M. Sprik, *ChemCatChem*, 2012, **4**, 636.
10 P. Salvador, *J. Phys. Chem. C*, 2007, **111**, 17038–17043.
11 P. Salvador, *Prog. Surf. Sci.*, 2011, **86**, 41–58.
12 H. Reiss, *J. Phys. Chem.*, 1985, **89**, 3783–3791.
13 Y. Tamaki, A. Furube, M. Murai, K. Hara, R. Katoh and M. Tachiya, *J. Am. Chem. Soc.*, 2006, **128**, 416–417.
14 D. Bahnemann, M. Hilgendorff and R. Memming, *J. Phys. Chem. B*, 1997, **101**, 4265–4275.
15 M. Murai, Y. Tamaki, A. Furube, K. Hara and R. Katoh, *Catal. Today*, 2007, **120**, 214–219.
16 J. Tang, J. R. Durrant and D. R. Klug, *J. Am. Chem. Soc.*, 2008, **130**, 13885–13891.
17 E. Bae and T. Ohno, *Appl. Catal., B*, 2009, **91**, 634–639.
18 T. Ohno, K. Sarukawa and M. Matsumura, *New J. Chem.*, 2002, **26**, 1167–1170.
19 T. Kisumi, A. Tsujiko, K. Murakoshi and Y. Nakato, *J. Electroanal. Chem.*, 2003, **545**, 99–107.
20 D. Lawless, N. Serpone and D. Meisel, *J. Phys. Chem.*, 1991, **95**, 5166–5170.
21 S. Tojo, T. Tachikawa, M. Fujitsuka and T. Majima, *Phys. Chem. Chem. Phys.*, 2004, **6**, 960–964.
22 A. Hagfeldt, U. Bjorksten and M. Gratzel, *J. Phys. Chem.*, 1996, **100**, 8045–8048.
23 B. Gregg, S. Chen and S. Ferrere, *J. Phys. Chem. B*, 2003, **107**, 3019–3029.
24 H. J. Snaith and M. Gratzel, *Adv. Mater.*, 2006, **18**, 1910.
25 J. Bisquert, G. Garcia-Belmonte and F. Fabregat-Santiago, *J. Solid State Electrochem.*, 1999, **3**, 337–347.
26 Y. K. Kho, A. Iwase, W. Y. Teoh, L. Maedler, A. Kudo and R. Amal, *J. Phys. Chem. C*, 2010, **114**, 2821–2829.
27 D. Hurum, A. Agrios, K. Gray, T. Rajh and M. Thurnauer, *J. Phys. Chem. B*, 2003, **107**, 4545–4549.
28 F. J. Knorr, C. C. Mercado and J. L. McHale, *J. Phys. Chem. C*, 2008, **112**, 12786–12794.
29 T. Kawahara, Y. Konishi, H. Tada, N. Tohge, J. Nishii and S. Ito, *Angew. Chem., Int. Ed.*, 2002, **41**, 2811.
30 X. Zhang, Y. Lin, D. He, J. Zhang, Z. Fan and T. Xie, *Chem. Phys. Lett.*, 2011, **504**, 71–75.
31 E. Borgarello, J. Kiwi, E. Pelizzetti, M. Visca and M. Gratzel, *Nature*, 1981, **289**, 158–160.
32 J. Enkovaara, C. Rostgaard, J. J. Mortensen, J. Chen, M. Dulak, L. Ferrighi, J. Gavnholt, C. Glinsvad, V. Haikola, H. A. Hansen, H. H. Kristoffersen, M. Kuisma, A. H. Larsen, L. Lehtovaara, M. Ljungberg, O. Lopez-Acevedo, P. G. Moses, J. Ojanen, T. Olsen, V. Petzold, N. A. Romero, J. Stausholm-Moller, M. Strange, G. A. Tritsaris, M. Vanin, M. Walter, B. Hammer, H. Hakkinen, G. K. H. Madsen, R. M. Nieminen, J. K. Norskov, M. Puska, T. T. Rantala, J. Schiotz, K. S. Thygesen and K. W. Jacobsen, *J. Phys.: Condens. Matter*, 2010, **22**, 253202.
33 B. Hammer, L. B. Hansen and J. K. Norskov, *Phys. Rev. B: Condens. Matter Mater. Phys.*, 1999, **59**, 7413.
34 A. Ruzsinszky, J. P. Perdew, G. I. Csonka, O. A. Vydrov and G. E. Scuseria, *J. Chem. Phys.*, 2007, **126**, 104102.
35 P. Mori-Sanchez, A. J. Cohen and W. Yang, *Phys. Rev. Lett.*, 2008, **100**, 146401.

This journal is © The Royal Society of Chemistry 2012

Energy Environ. Sci., 2012, **5**, 9866–9869 | 9869